American Society for Composites, 15th Annual Technical Conference
Texas A&M University, September 2000.

Modeling the Mechanical Interlocking between FRP Reinforcing Bars and Concrete

Jun Guo [1] and James V. Cox [1]

ABSTRACT

The use of fiber-reinforced polymer (FRP) bars to reinforced concrete is an application of composite material that has significant potential but still merits further investigation. For reinforcing bars with a significant surface structure (i.e., ribs), the mechanical interlocking between the surface structure and adjacent concrete can dominate the mechanical interaction, commonly called the *bond behavior*. This study focuses upon modeling the progressive failure of the surface structure of the bar — an issue unique to FRP reinforcing bars. The method of cells is adopted in combination with constitutive models for the polymer matrix, fibers, and their interaction. An elastoplastic-damage model within the framework of continuum damage mechanics is adopted to characterize the plastic and damage behavior of the matrix and fibers. The fiber-matrix interaction is treated with an "adhesive interface model" in which the breakdown of adhesion is defined in terms of a simple energy criterion. A slideline representation is used to characterize the rebar-concrete contact condition. Preliminary results using the model show good agreement with selected experimental data. The elastoplastic-damage model gives qualitatively correct predictions of the distribution of surface structure damage. The slideline representation appears to give reasonable predictions of how the mechanical interlocking produces contact along the surface structure. Additional work is still needed to address calibration of the constitutive models and localization within the FRP.

INTRODUCTION

In recently years there has been an increased interest in applying composite materials to infrastructure problems. Some applications of composite materials in infrastructure may only require a transfer of technology, but other applications present unique technical issues that merit additional research. One such application is reinforcing concrete with fiber-reinforced polymer (FRP) bars. Most of the early studies on this problem were experimental and examined the behavior of complete structures or their components. As with any reinforced system, the mechanical

[1] Department of Civil Engineering, Johns Hopkins University, Baltimore, MD 21218.

interaction between the two constituents (FRP and concrete), commonly called the *bond* behavior, has a significant effect upon the structural behavior. Many experimental bond studies have been conducted over the last ten years for a variety of different bars, but modeling efforts to both quantify the structural behavior and the underlying mechanisms that produce this behavior have been much more limited.

In this study we focus upon bars which have a significant *surface structure*, such that mechanical interlocking between the surface structure and the adjacent concrete dominates the mechanical interaction. The study also focuses upon smaller scale models that explicitly represent the surface structure of the bar (so called "rib-scale model" [1]) and thus can potentially characterize the underlying mechanisms that produce the "structural bond behavior". Models at this scale could potentially be used in "optimizing" the surface structure of the FRP bars.

Previous modeling efforts at this scale for FRP bars [1] have not focused on the progressive failure of the constituent materials; in most cases the materials have been treated as linear elastic. Apparently the first rib-scale analyses for FRP bars were conducted by Yonezawa et al. [2]. They performed "two dimensional plane analyses" of bars, examining the effects of various parameters upon bond. Their analyses were linear, thus to account for the concentration of force transfer across the bearing faces of the ribs, they reduced the Young's modulus in one layer of concrete elements adjacent to the other regions of the interface. Uppuluri et al. [3] developed some axisymmetric rib-scale models of a few different bars. For their models of commercial bars the concrete and FRP core were modeled as linear elastic. A resin-rich outer layer of the bar was modeled as elastic perfectly-plastic, and the analysis was halted at the initiation of plastic behavior. Slideline elements without friction were used to represent the contact between the bar and concrete.

The work presented here emphasizes the constitutive modeling of the FRP. The method of cells [4] for modeling the FRP and continuum damage mechanics (CDM) for characterizing plasticity and damage of the constituent materials are combined to model the progressive failure of the surface structure of the bar – an issue unique to FRP reinforcing bars. A slideline element approach was applied to characterize the large slip of the concrete-rebar interface. The following sections present an overview of the modeling and some numerical examples. Additional details are given in reference [5].

METHOD OF CELLS

The method of cells [4] is a micro-mechanical model for predicting the overall response of composites from the constitutive properties of their components. Fibers are assumed to be distributed regularly in the matrix so that it is sufficient to analyze the behavior of a single rectangular representative volume element (RVE). This single repeating element is further divided into subcells. Each subcell follows its own constitutive relation. In this study, the RVE consists of one fiber subcell, three matrix subcells, and two interface cells (Figure 1). The formulation follows the approach in [4] but is omitted here for brevity.

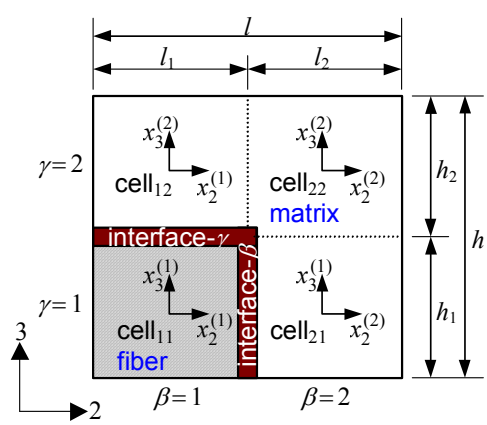

Figure 1. Subcells of an RVE

COUPLED ELASTOPLASTIC-DAMAGE MODEL

The elastoplastic-damage model for fiber and matrix was developed using the continuum damage mechanics based on irreversible thermodynamics with internal variables (see e.g., [6,7]). In addition to the strain components $\boldsymbol{\varepsilon}^e$ and $\boldsymbol{\varepsilon}^p$, the following internal variables were introduced: r – scalar isotropic hardening variable of plasticity, $\mathbf{D}$ – damage tensor, and β – scalar corresponding to the isotropic hardening of damage. We assume that the Helmholtz free energy (ψ) can be decomposed into an elastic potential (W), a plastic potential (ψ^p), and a damage potential (ψ^d) as,

$$\psi(\boldsymbol{\varepsilon}^e, \mathbf{D}, \boldsymbol{\alpha}, r, \beta) = W(\boldsymbol{\varepsilon}^e, \mathbf{D}) + \psi^p(r) + \psi^d(\beta) \tag{1}$$

A general form of $W(\boldsymbol{\varepsilon}^e, \mathbf{D})$ could be expressed as the combination of the direct or mixed invariants of $\boldsymbol{\varepsilon}^e$ and $\mathbf{D}$. The following form was used in this study and its variations and extensions have been widely used (see e.g., [8]):

$$W(\boldsymbol{\varepsilon}^e, \mathbf{D}) = 0.5\lambda(\mathrm{tr}\boldsymbol{\varepsilon}^e)^2 + \mu(\mathrm{tr}\boldsymbol{\varepsilon}^{e\,2}) + \theta_1 \mathrm{tr}\mathbf{D}\,(\mathrm{tr}\boldsymbol{\varepsilon}^e)^2 + \theta_4 \mathrm{tr}(\boldsymbol{\varepsilon}^e \mathbf{D} \boldsymbol{\varepsilon}^e) \tag{2}$$

where, tr(.) denotes the trace of a tensor, λ and μ are the Lame constants for the initial undamaged state, while θ_1 and θ_4 are material constants.

$\psi^p(r)$ and $\psi^d(\beta)$ are chosen to have the following forms (see e.g., [7,8]):

$$\psi^p(r) = \frac{R_\infty}{b}\left[br + \exp(-br)\right], \qquad \psi^d(\beta) = \frac{1}{2}K_\beta \beta^2 \tag{3,4}$$

where R_∞, b, and K_β are model parameters. The above form of ψ^p can result in an isotropic hardening stress which increases with r and tends to saturate to some value, whick is consistent with experimental observation of polymer materials.

The conjugate thermodynamic forces can be obtained by taking the derivatives of ψ with respect to the thermodynamic state variables as:

$$\boldsymbol{\sigma} = \frac{\partial W}{\partial \boldsymbol{\varepsilon}^e}, \qquad \mathbf{Y} = \frac{\partial W}{\partial \mathbf{D}}, \qquad R = \frac{\partial \psi^p}{\partial r}, \qquad B = \frac{\partial \psi^d}{\partial \beta} \tag{5}$$

Since damage will lead to the reduction of the actual load carrying area and induce stress concentrations around defects, the damage tensor $\mathbf{D}$ has been included in the yield function (F^p) and the following extended Drucker-Prager type yield function is assumed for elastoplastic-damage materials with isotropic hardening:

$$F^p(\boldsymbol{\sigma}, R; \mathbf{D}) = \sigma_{eq}(\boldsymbol{\sigma}; \mathbf{D}) + c^\sigma \mathrm{tr}(\boldsymbol{\sigma}) - (\sigma_0 + R) \tag{6}$$

where, σ_0 and c^σ are model parameters, and

$$\sigma_{eq} = \sqrt{\frac{3}{2}\boldsymbol{\sigma}' : \mathbf{M}(\mathbf{D}) : \boldsymbol{\sigma}'}, \qquad \mathbf{M}(\mathbf{D}) = \mathbf{I}_4 + c^p(\mathbf{I}_4\mathbf{D} + \mathbf{D}\mathbf{I}_4) \tag{7a,b}$$

" ' " represents a tensor's deviator, "**:**" denotes the contraction product to the second order of two tensors, $\mathbf{I}_4$ is the rank four symmetric identity tensor, c^p is a model parameter introducing the damage coupling. The incorporation of hydrostatic stress (tr($\boldsymbol{\sigma}$)) into the yield function is motivated by the experimental observation that the yielding of most polymers is pressure dependent.

Similar to the yield surface of plasticity, the damage surface describes the loading/unloading and neutral loading conditions. The following form is assumed for the damage function:

$$F^d(\mathbf{Y}, B; \mathbf{D}) = Y_{eq} - (B_0 + B) \tag{8}$$

$$Y_{eq} = \sqrt{\frac{1}{2}\mathbf{Y} : \mathbf{L}(\mathbf{D}) : \mathbf{Y}}, \qquad \mathbf{L}(\mathbf{D}) = \mathbf{I}_4 + c^d(\mathbf{I}_4\mathbf{D} + \mathbf{D}\mathbf{I}_4) \tag{9a,b}$$

where, B_0 and c^d are material constants, the former specifying the size of the initial damage surface. The form of $\mathbf{L}(\mathbf{D})$ is similar to the one proposed in [8].

In this study, the flow rule and evolution laws are assumed to be:

$$\dot{\boldsymbol{\varepsilon}}^p = \dot{\lambda}^p \frac{\partial F^p}{\partial \boldsymbol{\sigma}'}, \quad \dot{r} = \dot{\lambda}^p \frac{\partial F^p}{\partial(-R)} = \dot{\lambda}^p, \quad \dot{\mathbf{D}} = \dot{\lambda}^d \frac{\partial F^d}{\partial \mathbf{Y}}, \quad \dot{\beta} = \dot{\lambda}^d \frac{\partial F^d}{\partial(-B)} = \dot{\lambda}^d \quad (10)$$

where, $\dot{\lambda}^p$ and $\dot{\lambda}^d$ are the consistency parameters.

DAMAGE MODEL FOR FIBER-MATRIX INTERFACE

A simple micromechanical model for adhesive interfaces was adopted for the fiber-matrix interface. A traction-relative displacement relationship is used to represent the mechanical behavior of the interface. Both traction ($\boldsymbol{\sigma}$) and relative displacement ($\boldsymbol{\delta}$) have tangent and normal components, i.e., $\boldsymbol{\delta} = (\delta_t, \delta_n)$ and $\boldsymbol{\sigma} = (\sigma_t, \sigma_n)$. An elastic-frictional interface relation incorporating a damage measure (h) is proposed as

$$\sigma_n = K_n(h)\delta_n, \quad \sigma_t = K_t(h)\delta_t + c_f\langle -\sigma_n\rangle \operatorname{sgn}(\dot{\delta}_t) \quad (11a,b)$$

where K_t and K_n are the elastic stiffnesses in the tangent and normal directions, c_f is the coefficient of friction, and $\langle . \rangle$ is the Macauley bracket symbol. A simple power form was used to express K_t and K_n:

$$K_t(h) = K_{t0}(1-h)^{\alpha}, \quad K_n(h) = K_{n0}(1-h)^{\beta} \text{ when } \sigma_n > 0 \quad (12a,b)$$

where K_{t0}, K_{n0}, α, and β are model parameters.

A purely mechanical evolution equation for scalar damage h can be expressed in term of energy dissipated during the decohesion process as

$$\dot{h} = \frac{\langle \sigma_n \rangle \langle \dot{\delta}_n \rangle}{G_I} + \frac{\langle \sigma_t \dot{\delta}_t \rangle}{G_{II}} \quad (13)$$

where, G_I and G_{II} are mode-I and mode-II interface toughnesses, respectively. It is assumed that compressive normal stress has no contribution to interface degradation.

NUMERICAL EXAMPLES

This section presents numerical examples of the application of the rib-scale model to establish some of the capabilities and limitations of the approach. Numerical results were compared with experimental data, which were obtained from three studies. Figure 2 shows the sketches of FRP rebars employed in the experiments. Table I lists the specimen dimensions and material properties. Young's moduli and tensile strengths of concrete specimens were estimated from the empirical relations suggested by CEB if they are not provided [5]. As shown, the rebars considered here vary significantly in the pattern of surface deformation, material properties, and dimensions.

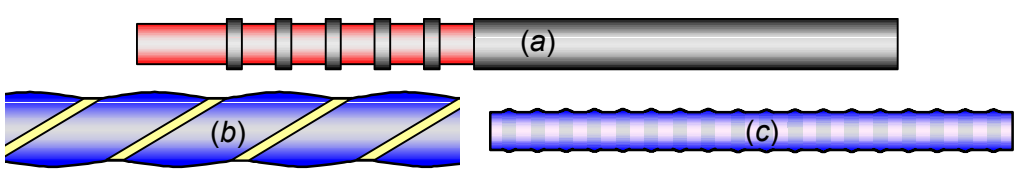

Figure 2. Sketches of FRP rebars used by three experimental studies: (*a*) Al-Zahrani [9], (*b*) Malvar [10], and (*c*) Cox et al. [11].

TABLE I. TEST SPECIMEN DATA AND MATERIAL PROPERTIES.

Experiment		Al-Zahrani et al.	Cox et al.	Malvar
Specimen size (mm)		150×150×150 (cube)	102×76 (cylinder)	102×76 (cylinder)
Bar diameter (mm)		10.1	10.5	19
Bond length (mm)		63.5	66.7	76.2
Surface ribs	Type Height (mm) Width (mm) Spacing (mm)	machined ribs 1.3 3.8, 8.9 12.7	molded ribs 0.63 3.7 7.63	indentation 1.75 30.2 34.3
Fiber	Young's modulus (GPa) Poisson's ratio Compressive strength (MPa)	85(G [1]), 220(C [2]) 0.2 3450(G), 3450(C)	–	88 0.2 3450
Matrix	Young's modulus (GPa) Poisson's ratio Compressive strength (MPa)	3.45(V [3]), 2.24(E [4]) 0.35 72(V), 123(E)	3.45 0.35 70	3.45 0.35 130
FRP [5]	Young's moduli (GPa) Shear's moduli (GPa) Poisson's ratios	–	119/7.51 3.74/2.74 0.27/0.31	–
Concrete	Young's modulus (GPa) Tensile strength (MPa) Compressive strength (MPa)	31.7, 35.5, 40.3 2.51, 3.35, 4.52 32, 45, 66	15.7 3.18 34.4	30.7 2.79 29.1

[1] Glass fiber [2] Carbon fiber [3] Vinyl ester [4] Epoxy
[5] The effective properties of the FRP bars in the longitudinal and transverse directions.

For all the three specimens, the following calibration values are used for the material parameters in the micromechanical model: $\theta_1=0.5\lambda$, $\theta_4=0.5\mu$, $b=4$, $K_\beta=50$, $c^\sigma=0.15$, $c^p=c^d=0$, $B_0=0.28$, $k_{n0}=200$GPa, $k_{t0}=100$GPa, $c_f=0.5$, $\alpha=\beta=2$, $G_I=50\text{kJm}^{-2}$, and $G_{II}=50\text{kJm}^{-2}$. Axisymmetric FEM models were used to model each specimen. A simple elastoplastic-damage model coupled with longitudinal cracks with softening was used to model the concrete in axisymmetric problems [5].

Al-Zahrani Tests

Al-Zahrani [9] conducted pullout tests on three types of FRP rebars: glass-vinyl ester (G/V), carbon-vinyl ester (C/V), and carbon-epoxy (C/E) FRP with

TABLE II. Summary of test and model results for the Al-Zahrani specimens.

FRP bars	Rib width (mm)	Concrete f_c (MPa)	Maximum shear stress (MPa)			
			Test	Model	% Diff.	Failure
G/V	3.8 3.8 3.8 8.9	45 31.4 66.1 45	39.7[1] 39.5 41.0 23.2[2]	40.8 40.3 43.0 29.3	3 % 2 % 5 % 26 %	Bar-rib Bar-rib Bar-rib Concrete
C/V	3.8	45	42.8[1]	41.7	3 %	Bar-rib
C/E	3.8	45	67.8[1]	70.7	4 %	Bar-rib

[1] Average of 3 tests. [2] Shear stress of concrete ribs instead of rebar ribs.

axisymmetric surface ribs which were fabricated by machining indentations into smooth bars. Different rib size and concrete were studied to investigate the effect of the rib width and concrete strength upon the mechanism of bond failure.

The FRP rebars were modeled with the elastoplastic-damage model of presented above. The interface between concrete and FRP rebars was modeled using an elastic-Coulomb friction model (friction coefficient $\mu = 0.49$, shear stiffness $k_t = 3{,}000$ N/mm^3, and compressive stiffness $k_n = 30{,}000$ N/mm^3).

For FRP bars with a rib width of 3.8 mm, both the experimental observations and model prediction show that all material systems experienced the same failure mode — shearing off of the FRP ribs. For the G/V bar with the rib width increased to 8.9 mm, both the experiment and the model indicate that the concrete now failed instead of the FRP. The numerical results are compared with the experimental data in Table II. The shear stress is defined as the pullout force divided by the total shear area of ribs.

Malvar Tests

Malvar [10] conducted experimental studies on the bond behavior of four different GFRP rebars with different surface structures. The experiment considered here is for the "type d" GFRP rebar. During the fabrication of the bar, the surface tow is stressed so that helical indentations are obtained. The bars were subjected to normal tractions at five different levels of compression with normal intensity of 500, 1500, 2500, 3500 psi, and 4500 psi (i.e., 3.45, 10.3, 17.2, 24.1, and 31 MPa). Prior to performing the bond tests, the concrete cylinder was pre-split.

Concrete and FRP rebars were modeled in the same way as that for the Al-Zahrani specimens. The concrete-rebar interface was modeled using slideline elements and treated as a nonlinear frictional surface using the same interface stiffnesses as the previous model. Some of the material properties of the Malvar specimens are listed in Table I.

The model results are compared with the experimental results in Table III. The difference between test and model results is within 15%.

Cox et al. Tests

Cox et al. [11] conducted a series of bond tests on four different CFRP bars using the Malvar specimen. The bar examined here is the C-BAR rod containing carbon fibers. The bars were subjected to normal tractions at the lower four levels of compression listed above. Prior to performing the bond tests, the concrete cylinder was pre-split by using the standard split cylinder test. The concrete is lightweight incorporated expanded shale for the coarse and fine aggregate.

TABLE III. SUMMARY OF TEST AND MODEL RESULTS FOR THE MALVAR SPECIMENS.

Conf. stress	Max. shear stress (MPa)		
	Test	Model	% Diff.
500 psi	3.37	3.40	1 %
1500 psi	7.40	7.36	1 %
2500 psi	10.42	10.45	1 %
3500 psi	12.07	13.39	11 %
4500 psi	13.47	15.55	15 %

TABLE IV. SUMMARY OF TEST AND MODEL RESULTS FOR THE COX ET AL. SPECIMENS.

Conf. stress	Max. shear stress (MPa)		
	Test	Model	% Diff.
500 psi	4.38[1]	3.08	30 %
1500 psi	6.41[2]	6.39	1 %
2500 psi	8.16[2]	8.33	2 %
3500 psi	10.4[1]	10.3	1 %

[1] Average of 3 tests. [2] Average of 2 tests.

Concrete and the concrete-FRP interface were modeled in the same way as before. Behavior of the external molded ribs was modeled using the elastoplastic-damage model while the FRP core was idealized as being transversely isotropic and elastic.

The results for the numerical model are compared with the experimental results in Figure 3 and Table IV. The model successfully predicted the bond strengths at confinement stresses of 1500, 2500, and 3500 psi. The bond behavior predicted by the model tends to be more brittle than the test result.

Figure 4 shows four photographs of bar surface damage and corresponding model predictions of the rib damage for two tests. The ribs of the 500 psi specimen were only "slightly damaged", while the ribs were almost sheared off for the 2500 psi and 3500 psi specimens. The predicted inelastic deformation of specimens at the same level of rib-damage provides a measurement of the amount of surface failure. The model successfully predicts the increase in surface damage with an increase in confinement.

DISCUSS AND CONCLUSIONS

A rib-scale model was developed to characterize the bond behavior resulting from the mechanical interlocking between FRP reinforcement and the surrounding concrete. The FRP material behavior was modeled using the method of cells. The fiber and matrix cells were modeled using a continuum damage mechanics model. A micromechanical interface model was proposed for characterizing the behavior of the bar-concrete interface.

Numerical examples presented here considered three types of FRP bar with significantly different surface structures. Most of the predicted bond strengths were within 15 percent of the measured values. The rib-scale model successfully predicted the failure modes for specimens with machined ribs. The predicted

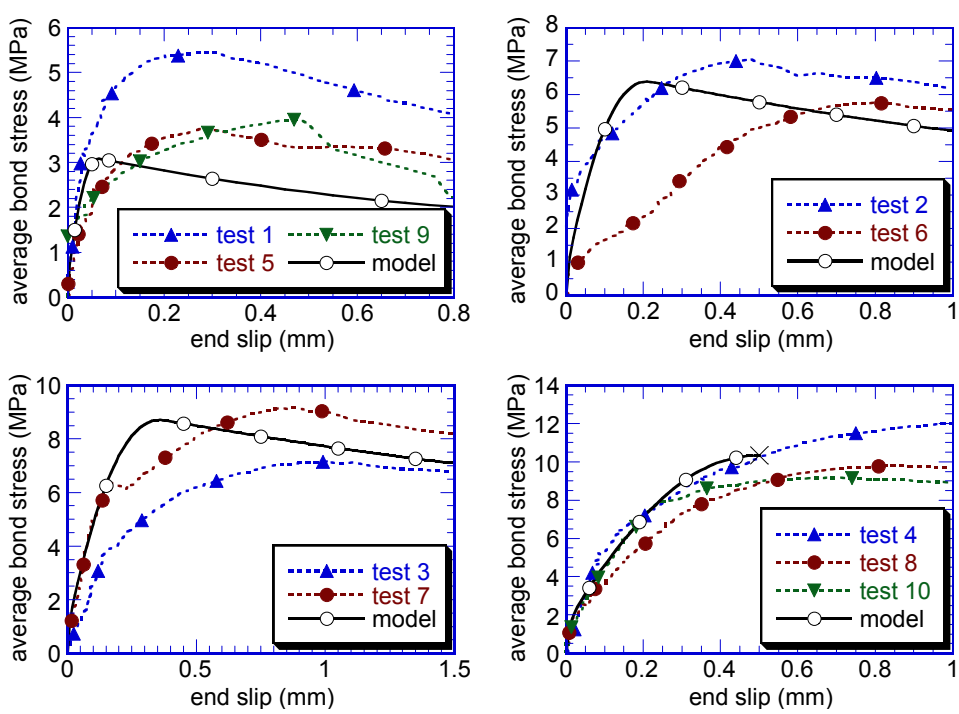

Figure 3. Bond stress vs. end slip for the Cox et al. [11] specimen.

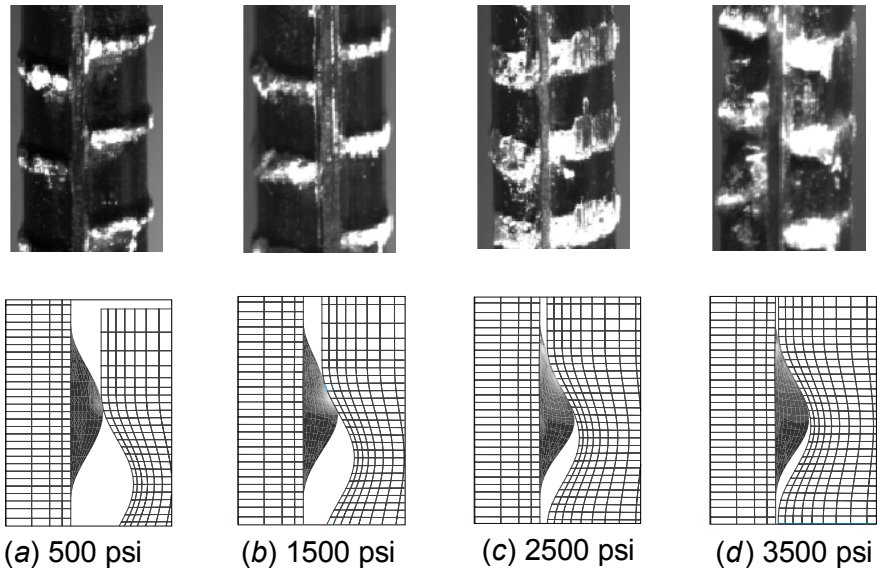

Figure 4. Deformation and surface damage ($\|\mathbf{D}\|_2$) of the bar rib.

surface damage for the bars having the molded ribs was qualitatively consistent with the experimental observation.

Additional work is still needed to address calibration of the constitutive models, localization within the FRP, and convergence problems when the constitutive models predict local crushing. Nonetheless, the initial results are encouraging and reflect the potential of using the model to predict bond strength and understand the contributions of mechanisms that affect the bond behavior up to rib failure.

ACKNOWLEDGEMENT

Support for this study by the National Science Foundation (grant no. CMS-9872609), Naval Facilities Engineering Service Center (contract no. N002499P2444), and the Office of Naval Research is gratefully acknowledged.

REFERENCES:

1. Cox, J.V.(1999). "Computational models for the bond between FRP reinforcing bars and concrete," *American Society for Composites' 14th Annual Technical Conference*, Dayton, OH. 10pp.
2. Yonezawa, T., S. Ohno, T. Kakizawa, K. Inoue, T. Fukata, and R. Okamoto (1993). "A new three-dimentional FRP reinforcement," *Fiber-Reinforced-Plastic (FRP) for Concrete Structures: Properties and Applications*, Nanni ed., Elsevier, pp. 405-418.
3. Uppuluri, V.S., C.E. Bakis, A. Nanni, and T.E. Boothby (1996). "Finite element modeling of the bond between fiber reinforced plastic (FRP) reinforcement and concrete," *Report CMTC-9602*, Composites Manufacturing Technology Center, Penn State University.
4. Aboudi, J. (1987). "Damage in composites - modeling of imperfect bonding," Composites Science and Technology, vol. 28, no. 2, pp. 103-128.
5. Guo, J. (2000). *Modeling the Mechanical Interaction between FRP Bars and Concrete*, Ph.D. Dissertation, Johns Hopkins University.

6. Coleman, B.D., and M.E. Gurtin (1967). "Thermodynamics with internal state variables," *Journal of Chemistry and Physics*. vol. 47, pp. 597-613.
7. Lemaitre, J. (1996). *A Course on Damage Mechanics*, Springer-Verlag
8. Hayakawa, K., and S. Murakami (1998). "Space of damage conjugate force and damage potential of elastic-plastic-damage materials," *Damage Mechanics in Engineering Materials*, Voyiadjis et al. ed., pp. 27-44.
9. Al-Zahrani, M.M. (1995). *Bond Behavior of Fiber Reinforced Plastic (FRP) Reinforcement with Concrete*, Ph.D. dissertation, The Pennsylvania State University.
10. Malvar, L.J. (1994). "Bond stress-slip characteristics of FRP rebars," *Technical Report TR-2013-SHR*, Naval Facilities Engineering Service Center.
11. Cox, J.V., K. Bergeron, and L.J. Malvar (2000). "A combined experimental and numerical study of the bond between lightweight concrete and CFRP bars," ASCE 14th EM Conference, Austin, Texas, CD